# Tellurium emission line in kilonova AT 2017gfo

Kenta Hotokezaka,[1][★] Masaomi Tanaka [ID],[2] Daiji Kato[3,4] and Gediminas Gaigalas[5]

[1]*Research Center for the Early Universe, Graduate School of Science, University of Tokyo, Bunkyo, Tokyo 113-0033, Japan*
[2]*Astronomical Institute, Tohoku University, Aoba, Sendai 980-8578, Japan*
[3]*National Institute for Fusion Science, 322-6 Oroshi-cho, Toki 509-5292, Japan*
[4]*Interdisciplinary Graduate School of Engineering Sciences, Kyushu University, Fukuoka 816-8580, Japan*
[5]*Institute of Theoretical Physics and Astronomy, Vilnius University, Saulėtekio Ave. 3, Vilnius 10222, Lithuania*

## ABSTRACT

The late-time spectra of the kilonova AT 2017gfo associated with GW170817 exhibit a strong emission line feature at 2.1 µm. The line structure develops with time and there is no blueshifted absorption feature in the spectra, suggesting that this emission line feature is produced by electron collision excitation. We attribute the emission line to a fine structure line of Tellurium (Te) III, which is one of the most abundant elements in the second r-process peak. By using a synthetic spectral modelling including fine structure emission lines with the solar r-process abundance pattern beyond the first r-process peak, i.e. atomic mass numbers $A \gtrsim 88$, we demonstrate that [Te III] 2.10 µm is indeed expected to be the strongest emission line in the near infrared region. We estimate that the required mass of Te III is $\sim 10^{-3}\,M_\odot$, corresponding to the merger ejecta of 0.05 $M_\odot$, which is in agreement with the mass estimated from the kilonova light curve.

**Key words:** neutron star mergers.

## 1 INTRODUCTION

The origin of r-process elements is a long-standing problem in astrophysics (Burbidge et al. 1957; Cameron 1957). Neutron star mergers have been considered as promising sites of r-process nucleosynthesis (Lattimer & Schramm 1974). A neutron star merger, GW170817, was accompanied by an uv–optical–infrared counterpart, a kilonova (or macronova) AT 2017gfo, which provides strong evidence that r-process nucleosynthesis occurs in neutron star merger ejecta (see, e.g. Metzger 2017; Nakar 2020; Margutti & Chornock 2021, for reviews).

A series of spectral data of the kilonova AT 2017gfo was obtained in the optical and near infrared bands from 0.5 to 10 d after the merger (Andreoni et al. 2017; Chornock et al. 2017; Kasliwal et al. 2017; Pian et al. 2017; Smartt et al. 2017; Tanvir et al. 2017; Troja et al. 2017). The kilonova AT 2017gfo is dominated by the photospheric emission at the early times. The emission around a few days after the merger peaks in the near infrared band, indicates the existence of lanthanides, which have strong absorption at optical to near infrared wavelengths (Barnes & Kasen 2013; Kasen, Badnell & Barnes 2013; Tanaka & Hotokezaka 2013; Kawaguchi, Shibata & Tanaka 2018; Fontes et al. 2020; Tanaka et al. 2020; Barnes et al. 2021). The early spectra also exhibit several absorption structures including: (i) the 0.8 µm feature attributed to Sr II or He I (Watson et al. 2019; Domoto et al. 2021; Gillanders et al. 2022; Perego et al. 2022; Tarumi et al. 2023) and (ii) the 1.3 µm and 1.5 µm features attributed to La III and Ce III, respectively (Domoto et al. 2022). In addition, Sneppen et al.

(2023) demonstrated that the spectra in this phase are useful to study the geometry of the outer part of the kilonova ejecta, $\gtrsim 0.2c$.

After the photospheric phase, kilonovae enter the nebula phase, where the ejecta is heated by charged decay products of the radioactivity of r-process nuclei and the heat is radiated through atomic emission lines. Examining kilonova nebular spectra provides opportunities to identify atomic species synthesized in the merger ejecta that may not appear as absorption lines during the photospheric phase. For instance, Hotokezaka et al. (2022) interpreted the detection of *Spitzer* (Villar et al. 2018; Kasliwal et al. 2022) at 4.5 µm at 43 and 74 d after the merger as emission lines of selenium (Se) or tungsten (W).

In the intermediate phase between the photospheric and nebular phases, $\sim 10$ d, the infrared emission is of particular interest because the absorption opacity due to atomic transitions is lower compared to the optical region (e.g. Tanaka et al. 2020), and thus, the emission lines are expected to appear as early as $\lesssim 10$ d. Most of infrared emission lines are expected to arise from fine-structure transitions in the ground terms of heavy elements, for which the line wavelengths and transition rates can be obtained with reasonably high accuracy from the experimentally calibrated atomic energy levels. Furthermore, such emission lines can be used to estimate the mass distribution of the emitting ions from the emission line spectra (see e.g. DerKacy et al. 2023; Kwok et al. 2023, for Type Ia supernova nebular emission).

In Section 2, we study an emission line feature at 2.1 µm in the kilonova AT 2017gfo spectra from 7.5 to 10.5 d. We attribute this line to a fine-structure line of doubly ionized Tellurium (Te III, atomic number 52). The Te III mass that is required to explain the observed data is estimated as $\sim 10^{-3}\,M_\odot$. With a synthetic spectral modelling with the solar r-process abundance pattern, we show that [Te III]

---

[★] E-mail: kentah@g.ecc.u-tokyo.ac.jp

2.10 μm is the strongest fine structure emission line in the near infrared region. In Section 3, we conclude the results and discuss the uncertainties and implications.

## 2 TE III LINE IN KILONOVA

The emission lines produced through radiative de-excitation of atoms emerge from the optically thin region of the ejecta. The optical depth of the kilonova ejecta with an expansion velocity of $v_{ej}$ and a mass of $M_{ej}$ is

$$\tau \approx \frac{\kappa M_{ej}}{4\pi (v_{ej}t)^2}, \tag{1}$$

$$\approx 1 \left(\frac{\kappa}{1\,\text{cm}^2\,\text{g}^{-1}}\right) \left(\frac{M_{ej}}{0.05\,\text{M}_\odot}\right) \left(\frac{v_{ej}}{0.1c}\right)^{-2} \left(\frac{t}{10\,\text{d}}\right)^{-2}, \tag{2}$$

where $\kappa$ is the opacity and $t$ is the time since merger. The opacity is dominated by bound–bound transitions of heavy elements and depends on the composition and wavelengths. Tanaka et al. (2020) show that the expansion opacity decreases with wavelength, e.g. $\sim 10$–$100\,\text{cm}^2\,\text{g}^{-1}$ around 0.5 μm and $\lesssim 1\,\text{cm}^2\,\text{g}^{-1}$ around 2 μm. Therefore, infrared emission lines are expected to emerge at the earlier time than optical lines. For AT 2017gfo, we expect emission lines to dominate over the photospheric emission as early as $\sim 10$ d around 2 μm.

Fig. 1 shows the spectral series of the kilonova AT 2017gfo from 7.5 to 10.5 d after the merger taken by X-shooter on the Very Large Telescope (Pian et al. 2017). The observed spectra are composed of several line features and a continuum component extending from the optical to near infrared bands. We model the underlying continuum spectrum by blackbody radiation, where the photospheric velocity and temperature for 7.5–10.5 d are 0.06–0.08$c$ and 1700–2400 K, respectively.

The observed spectra clearly show an emission line at 2.1 μm. The expansion velocity of the line emitting region is ∼0.07$c$ derived from Doppler broadening of the line, which is consistent with the picture where the emission line is produced outside the photosphere. The line flux remains roughly constant with time while the continuum flux declines, and thus, the line-to-continuum ratio increases from ∼1 at 7.5 d to ∼1.5 at 10.5 d. This development of the emission line without a blueshifted absorption feature indicates that the emission at 2.1 μm is a forbidden line driven by electron collision rather than an emission line associated with an absorption line, e.g. a P-Cygni line or a fluorescence line.

The wavelength of the peak of the emission line feature indeed coincides with a fine structure line, [Te III] 2.10 μm, arising from the transition between the ground level $^3P_0$ and the first excited level $^3P_1$. It is worth noting that [Te III] 2.10 μm has been detected in planetary nebulae (Madonna et al. 2018). Note that the transition between the ground level $^3P_2$ and the second excited level $^3P_1$ of Te I also produces an emission line at 2.1 $\mu m$. As discussed later, the contribution of Te I line is weaker than Te III line.

It may be not surprising that Te III produces the strongest emission lines because Te is among the most abundant elements in the second r-process peak. Fig. 2 shows the mass fraction of each atom at 10 d after the merger. Here, we assume that the final abundance pattern matches the solar r-process residual with atomic numbers $A \geq 88$ (Hotokezaka & Nakar 2020), i.e. the elements beyond the first r-process peak. With this assumption, the most abundant element is Sr and the second most is Te at 10 d.

Note also that [Te III] 2.10 μm is particularly expected to be strong as long as Te III is abundant outside the photosphere because this line is produced by radiative decay of the first fine structure level, which
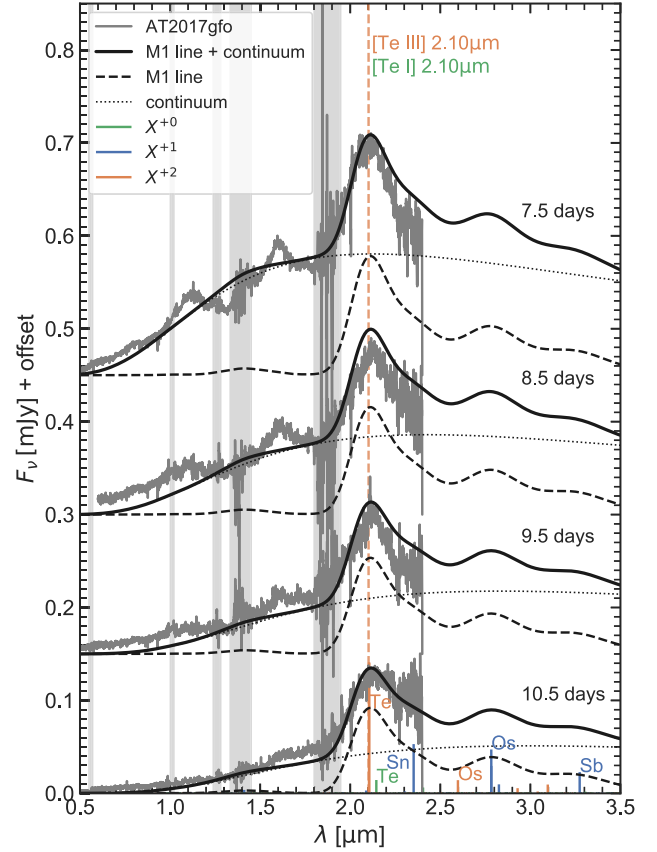


**Figure 1.** Spectral series of the kilonova AT 2017gfo 7.5–10.5 d after the merger. The observed data were taken by X-shooter on VLT (Pian et al. 2017). The synthetic spectra are composed of fine structure emission lines (dashed curve) and a continuum (dotted curve), where the continuum emission is approximate by a blackbody with temperatures $T_{BB} = 2400, 2100, 1800, 1700$ K at 7.5, 8.5, 9.5 and 10.5 d, respectively. The electron temperature is fixed to be 2000 K. The ejecta model assumes $M_{ej} = 0.05\,\text{M}_\odot$, $v_{exp} = 0.07c$, and $n_e = 10^7\,\text{cm}^{-3}(t/9.5\,\text{d})^{-3}$. We use ionization fractions of ($Y^{+0}$, $Y^{+1}$, $Y^{+2}$, $Y^{\geq+3}$) = (0.25 0.4, 0.25, 0.1) for all the atomic species for simplicity. The composition is assumed to be the solar r-process abundance pattern with $A \geq 88$ (Fig. 2). The shape of each emission line is assumed to be a Gaussian profile with a broadening parameter of 0.07$c$. The distance to the source is set to = 40 Mpc. The wavelength of [Te I] 2.10 μm and [Te III] 2.10 μm is shown as a vertical dashed line. Also shown as vertical lines are possibly strong emission lines at 10.5 d. The grey shaded vertical regions depict the wavelength ranges between the atmospheric windows. The wavelength of [Te I] 2.10 μm is shown with an offset of +0.04 μm.

is easily excited by electron collision. For the iron peak elements, [Co III] 11.89 μm and [Co II] 10.52 μm represent lines of the same nature. Indeed, these are among the most prominent mid-IR lines observed in SNe Ia and SN 1987A, respectively (e.g. Wooden et al. 1993; Kwok et al. 2023).

Let us first give an estimate of the amount of Te III from the observed line flux by assuming that the observed line flux is predominantly produced by Te III and the ejecta is optically thin to the [Te III] 2.10 μm. The total line luminosity is given by ###

$$L \sim h\nu_{10} A_{10} f_1 N(\text{Te III}), \tag{3}$$

where $h\nu_{10}$, $A_{10} \approx 2\,\text{s}^{-1}$, and $f_1$ are the excitation energy, the radiative decay rate, and the fraction of Te III ions in the $^3P_1$ level, respectively, and $N(\text{Te III})$ is the total number of Te III ions in the ejecta (see
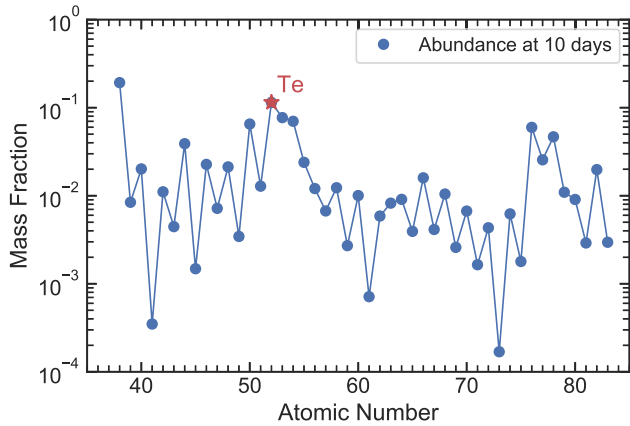
**Figure 2.** Elemental mass fraction used in the synthetic modelling. The abundance pattern at 10 d is determined such that the final abundance pattern at $\sim 5$ Gyr matches the solar r-process residual for $88 \leq A \leq 209$. Tellurium is the second most abundant element in this model.

equations 1 and 2 in Hotokezaka et al. 2022, for the formula of M1 transition probabilities). The observed flux at 2.1 μm after subtracting the underlying continuum is $\sim 0.1$ mJy, corresponding to the observed line luminosity of $L_{\rm obs,line} \sim 2 \times 10^{39}$ erg s$^{-1}$ with $D = 40$ Mpc. Equation (3) leads to a total mass of Te III:

$$M(\text{Te III}) \sim 10^{-3}\,\text{M}_\odot \left(\frac{f_1}{0.1}\right)^{-1} \left(\frac{L_{\rm obs,line}}{2 \times 10^{39}\,\text{erg s}^{-1}}\right). \quad (4)$$

Note that the electron density at $t \sim 10.5$ d may be comparable to the critical density of Te III $^3P_1$ (Madonna et al. 2018), and therefore, the level fraction $f_1$ is comparable to or slightly less than that expected from the thermal distribution, i.e. $f_1 \approx 0.1$ in thermal equilibrium at $T_{\rm e} = 2000$ K. Given the total ejecta mass of $\sim 0.05$ M$_\odot$, we estimate that the mass fraction of Te is greater than a few per cent.

We now turn to the comparison of the observed spectra with a synthetic spectral model. The synthetic spectrum is composed of fine structure emission lines and a continuum component, where the continuum emission is approximated by blackbody radiation. The blackbody temperature and radius at a given epoch are determined such that the synthetic spectrum roughly agrees with the observed one at the near IR region $\lesssim 2$ μm.

The emission line spectrum is computed by the one-zone modelling presented in Hotokezaka et al. (2022), where the energy level populations are solved by balance between collision and radiative decay for a given electron density, temperature, and ionization state. We use the collision strengths of the fine structure transitions of the ground term of Te III derived by Madonna et al. (2018). The collision strengths of other elements that are relevant for the nebular modelling at $\lambda \lesssim 3.5$ μm are obtained by using an atomic structure code HULLAC (Bar-Shalom, Klapisch & Oreg 2001; see also Hotokezaka et al. 2022) and the M1 line list is constructed by using the NIST data base (Kramida et al. 2021) and the LS selection rules with the single-configuration approximation. Note that the wavelengths and radiative transition rates of the M1 lines in the list are sufficiently accurate for our purpose.

In the modelling, the ejecta composition is assumed to be the solar r-process abundance pattern with $A \geq 88$ (Fig. 2). The ionization fractions are $(Y^{+0}, Y^{+1}, Y^{+2}, Y^{\geq +3}) = (0.25, 0.4, 0.25, 0.1)$.[1] This choice is motivated by Pognan, Jerkstrand & Grumer (2022a), where

the ionization fractions of Te atoms in the kilonova nebular phase are studied. A caveat here is that the ionization fraction should vary among different atomic species. Note that, however, the singly and doubly ionized ions are typically the most and second most abundant around 10 d (Hotokezaka et al. 2021; Pognan et al. 2022a).

We choose the electron temperature to be $T_{\rm e} = 2000$ K. Furthermore, $T_{\rm e}$ is assumed to be constant with time because of the following reason. In the line forming region, $T_{\rm e}$ is determined by the balance between the line cooling and radioactive heating. The former is given by equation (3), where $f_1$ obeys the Boltzmann distribution for $n_{\rm e} \gg n_{\rm c}$ and decreases as $n_{\rm e} \propto t^{-3}$ for $n_{\rm e} \ll n_{\rm c}$. Here, $n_{\rm c} \approx 6 \times 10^6$ cm$^{-3}$ is the critical density of the first excited level of Te III. Given the time dependence of the heating rate $\propto t^{-1.3}$ (Metzger et al. 2010), $T_{\rm e}$ decreases and increases with time for $n_{\rm e} \gg n_{\rm c}$ and $n_{\rm e} \ll n_{\rm c}$, respectively. Because $n_{\rm e}$ is roughly $n_{\rm c}$ for 7.5–10.5 d, $T_{\rm e}$ is expected to be roughly constant with time if the [Te III] line dominates the cooling in the line forming region.

With these choices of the ionization and $T_{\rm e}$, the ejecta mass of 0.05 M$_\odot$, and the expansion velocity of $0.07c$, [Te III] 2.10 μm is the strongest emission line among M1 transitions of all the heavy elements beyond the first r-process peak and the synthetic spectra can roughly reproduce the emission line structure around 2.1 μm. The ejecta mass of 0.05 M$_\odot$ agrees with the ejecta mass estimated from the energy budget of the bolometric light curve (Kasen & Barnes 2019; Waxman, Ofek & Kushnir 2019; Hotokezaka & Nakar 2020).

If this interpretation is correct, we expect that the 2.1 μm line remains at the later times while the continuum flux keeps declining. It is worth noting that Te III may produce another emission line at 2.93 μm arising from the transition between the first and second excited levels ($^3P_1$–$^3P_2$) at the later times because the electron temperature is expected to gradually increase with time (Hotokezaka et al. 2021; Pognan et al. 2022a). Although this line may be hidden by several other lines of Os II, III, and Pd III, detecting the two lines of Te III in future events can provide solid confirmation of the Te III production in mergers. Furthermore, the ratio of these line fluxes can be used to diagnose the electron temperature.

## 3 CONCLUSION AND DISCUSSION

The observed spectra of the kilonova AT 2017gfo exhibit a strong emission line at 2.1 μm. The emission line with the lack of an apparent blueshifted absorption feature and the strong excess from the continuum suggest that the emission feature is a forbidden line excited through electron collision. We attribute this line to the fine structure line, [Te III] 2.10 μm, which has also been detected in planetary nebulae (Madonna et al. 2018). Note that Te is one of the most abundant elements in the second r-process peak. We estimate that the mass of Te III is roughly $10^{-3}$ M$_\odot$ to account for the observed line flux.

We compare the observed spectra with a synthetic model, where the spectrum is composed of emission lines and a continuum component approximated by blackbody radiation. The spectrum of fine structure emission lines is computed with the one-zone model presented in Hotokezaka et al. (2022). With the solar r-process abundance beyond the first r-process peak, $T_{\rm e} \sim 2000$ K, and $Y^{+2} \sim 0.3$, we show that [Te III] 2.10 μm is the strongest emission line among M1 transitions of all the heavy elements around 10 d after merger. Our model agrees with the observed spectra for the ejecta of 0.05 M$_\odot$ with the solar r-process abundance pattern with $A \geq 88$, an expansion velocity of $0.07c$, and electron temperature of $\sim 2000$ K, and the ionization fraction of $Y^{+2} \sim 0.3$. Because blackbody radiation may be a poor approximation to the continuum flux around 2 μm we

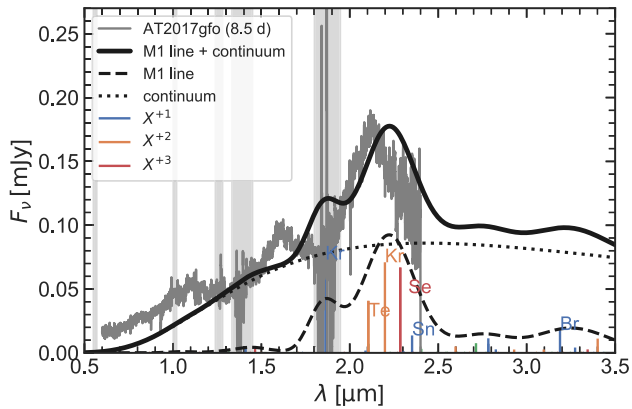[1]We neglect the emission lines of ions in $Y^{\geq +3}$.

**Figure 3.** The same as Fig. 1 but the first peak elements $69 \leq A \leq 87$ are included according to the solar r-process abundance pattern. The electron temperature is set to be 2500 K and the electron density is twice the value used for Fig. 1. While [Kr III] 2.20 μm and [Se IV] 2.29 μm dominate the flux, the wavelengths of the lines are too long to reproduce the observed feature.

should keep in mind that the amount of Te III in our analysis may be affected by the continuum flux model.

It is also interesting to note that the same abundance pattern can reproduce the *Spitzer* 4.5 μm detection at 40 d (Villar et al. 2018; Kasliwal et al. 2022), in which the emission is attributed to a fine structure line of W III (Hotokezaka et al. 2022). Note that, if the lighter r-process elements are abundant, they are expected to produce emission lines around 2 μm such as [Kr III] 2.20 μm and [Se IIV] 2.29 μm (see Fig. 3). However, the observed spectra peak at 2.1 μm, suggesting that these ions are less abundant relative to Te III in the line emitting region of the ejecta.

Our model does not include electric dipole (E1) lines, which may produce strong absorption and emission lines. Recently, Gillanders et al. (2023) suggested that 2.1 μm may be composed of two lines and an E1 line of Ce III is the best candidate producing this line feature. Although we cannot quantify the contribution of E1 lines to the 2.1 μm feature, we emphasize that the M1 emission of Te can produce the observed line flux with the reasonable parameters. To verify this hypothesis we need spectral modellings with E1 lines.

We also note that the M1 lines in our list cannot account for the observed feature at 1.6 μm. The flux in this line declines with time as the continuum flux declines, indicating that this emission feature may be produced by E1 lines. Interestingly, Domoto et al. (2022) show that Ce III has several strong E1 lines around 1.6 μm.

From the early blue emission in the photospheric phase, it is suggested that the emission is dominated by the ejecta composed of light r-process elements in order to avoid significant absorption by lanthanides in the optical band. Furthermore, the analyses of the kilonova spectra in the photospheric phase lead to the similar conclusion. The absorption feature around 0.8 μm is likely caused by one of light r-process elements, Sr ($Z = 38$), or even He (Watson et al. 2019; Gillanders et al. 2022; Tarumi et al. 2023). Domoto et al. (2022) propose that La ($Z = 57$) and Ce ($Z = 58$) produce the absorption lines around 1.2 and 1.5 μm, respectively. But the abundances of La and Ce inferred from the spectral analysis are lower than the solar r-process residuals by factor of ∼10. These indicate that the outer part of the ejecta ($v \gtrsim 0.2c$) is predominantly composed of light r-process elements. In contrast to the early emission, our analysis implies that heavier elements, i.e. the second r-process peak, are likely more abundant in the slower part of the ejecta.

In order to obtain better constraints on the elemental abundances and ejecta parameters, the spectral modellings should be improved by developing non-LTE radiation transfer modellings (e.g. Pognan, Jerkstrand & Grumer 2022b) and by improving atomic data such as the radiative transition rates (e.g. Gaigalas et al. 2019), collision strengths, and recombination rate coefficients. For future kilonova events, the spectroscopic observations with the JWST as well as ground-based telescopes will be useful to identify more elements in the nebular spectra with a wider wavelength range.

## DATA AVAILABILITY

The data presented this article will be shared on request to the corresponding author.

## REFERENCES

Andreoni I. et al., 2017, PASA, 34, e069
Bar-Shalom A., Klapisch M., Oreg J., 2001, J. Quant. Spectrosc. Radiat. Transfer, 71, 169
Barnes J., Kasen D., 2013, ApJ, 775, 18
Barnes J., Zhu Y. L., Lund K. A., Sprouse T. M., Vassh N., McLaughlin G. C., Mumpower M. R., Surman R., 2021, ApJ, 918, 44
Burbidge E. M., Burbidge G. R., Fowler W. A., Hoyle F., 1957, Rev. Mod. Phys., 29, 547
Cameron A. G. W., 1957, PASP, 69, 201
Chornock R. et al., 2017, ApJ, 848, L19
DerKacy J. M. et al., 2023, ApJ, 945, L2
Domoto N., Tanaka M., Wanajo S., Kawaguchi K., 2021, ApJ, 913, 26
Domoto N., Tanaka M., Kato D., Kawaguchi K., Hotokezaka K., Wanajo S., 2022, ApJ, 939, 8
Fontes C. J., Fryer C. L., Hungerford A. L., Wollaeger R. T., Korobkin O., 2020, MNRAS, 493, 4143
Gaigalas G., Kato D., Rynkun P., Radžiūtė L., Tanaka M., 2019, ApJS, 240, 29
Gillanders J. H., Smartt S. J., Sim S. A., Bauswein A., Goriely S., 2022, MNRAS, 515, 631
Gillanders J. H., Sim S. A., Smartt S. J., Goriely S., Bauswein A., 2023, preprint (arXiv:2306.15055)
Hotokezaka K., Nakar E., 2020, ApJ, 891, 152
Hotokezaka K., Tanaka M., Kato D., Gaigalas G., 2021, MNRAS, 506, 5863
Hotokezaka K., Tanaka M., Kato D., Gaigalas G., 2022, MNRAS, 515, L89
Kasen D., Barnes J., 2019, ApJ, 876, 128
Kasen D., Badnell N. R., Barnes J., 2013, ApJ, 774, 25
Kasliwal M. M. et al., 2017, Science, 358, 1559
Kasliwal M. M. et al., 2022, MNRAS, 510, L7
Kawaguchi K., Shibata M., Tanaka M., 2018, ApJ, 865, L21
Kramida A., Ralchenko Yu., Reader J., NIST ASD Team, 2021, NIST Atomic Spectra Database, Version 5.9, doi: https://physics.nist.gov/asd, (accessed 9 April 2017)
Kwok L. A. et al., 2023, ApJ, 944, L3
Lattimer J. M., Schramm D. N., 1974, ApJ, 192, L145
Madonna S. et al., 2018, ApJ, 861, L8
Margutti R., Chornock R., 2021, ARA&A, 59
Metzger B. D., 2017, Living Rev. Relativ., 20, 3

Metzger B. D. et al., 2010, MNRAS, 406, 2650

Nakar E., 2020, Phys. Rep., 886, 1

Perego A. et al., 2022, ApJ, 925, 22

Pian E. et al., 2017, Nature, 551, 67

Pognan Q., Jerkstrand A., Grumer J., 2022a, MNRAS, 510, 3806

Pognan Q., Jerkstrand A., Grumer J., 2022b, MNRAS, 513, 5174

Smartt S. J. et al., 2017, Nature, 551, 75

Sneppen A., Watson D., Bauswein A., Just O., Kotak R., Nakar E., Poznanski D., Sim S., 2023, Nature, 614, 436

Tanaka M., Hotokezaka K., 2013, ApJ, 775, 113

Tanaka M., Kato D., Gaigalas G., Kawaguchi K., 2020, MNRAS, 496, 1369

Tanvir N. R. et al., 2017, ApJ, 848, L27

Tarumi Y., Hotokezaka K., Domoto N., Tanaka M., 2023, preprint (arXiv:2302.13061)

Troja E. et al., 2017, Nature, 551, 71

Villar V. A. et al., 2018, ApJ, 862, L11

Watson D. et al., 2019, Nature, 574, 497

Waxman E., Ofek E. O., Kushnir D., 2019, ApJ, 878, 93

Wooden D. H., Rank D. M., Bregman J. D., Witteborn F. C., Tielens A. G. G. M., Cohen M., Pinto P. A., Axelrod T. S., 1993, ApJS, 88, 477

This paper has been typeset from a T<sub>E</sub>X/L<sup>A</sup>T<sub>E</sub>X file prepared by the author.